Ion-dust streaming instability with non-Maxwellian ions

Hanno Kählert

Citation: Physics of Plasmas **22**, 073703 (2015); doi: 10.1063/1.4926531
View online: http://dx.doi.org/10.1063/1.4926531
View Table of Contents: http://scitation.aip.org/content/aip/journal/pop/22/7?ver=pdfcov
Published by the AIP Publishing

Ion-dust streaming instability with non-Maxwellian ions

Hanno Kählert[a)]
Institut für Theoretische Physik und Astrophysik, Christian-Albrechts-Universität zu Kiel, Leibnizstr. 15, 24098 Kiel, Germany

(Received 8 April 2015; accepted 25 June 2015; published online 13 July 2015)

The influence of non-Maxwellian ions on the ion-dust streaming instability in a complex plasma is investigated. The ion susceptibility employed for the calculations self-consistently accounts for the acceleration of the ions by a homogeneous background electric field and their collisions with neutral gas particles via a Bhatnagar-Gross-Krook collision term [e.g., A. V. Ivlev *et al.*, Phys. Rev. E **71**, 016405 (2005)], leading to significant deviations from a shifted Maxwellian distribution. The dispersion relation and the properties of the most unstable mode are studied in detail and compared with the Maxwellian case. The largest deviations occur at low to intermediate ion-neutral damping. In particular, the growth rate of the instability for ion streaming below the Bohm speed is found to be lower than in the case of Maxwellian ions, yet remains on a significant level even for fast ion flows above the Bohm speed. © *2015 AIP Publishing LLC*. [http://dx.doi.org/10.1063/1.4926531]

I. INTRODUCTION

Dust density or dust acoustic waves[1] are among the basic dynamic phenomena that can be observed in extended dust clouds in complex plasmas,[2–12] see Ref. 13 for a recent review. Shielding by the light ions and electrons leads to an acoustic type wave with a phase velocity on the order of a few cm/s,[13] which can be regarded as the analog of an ion-acoustic wave in an electron-ion plasma. Dust density waves can be excited as a result of an ion-dust streaming instability, which has been investigated with diverse methods, e.g., fluid[6,9,14–17] and kinetic theory[3,4,18–22] or computer simulations.[23,24] It was found that even moderate ion flows are sufficient to generate the instability, provided dust-neutral damping is low.[13]

Kinetic models of the ion-dust streaming instability were mostly based on shifted Maxwellian (MW) distribution functions for the ions.[3,4,18–22,25] However, it was shown that in situations where the ion flow is caused by externally imposed electric fields and when ion-neutral collisions are important, as is often the case in complex plasmas, substantial deviations from a shifted Maxwellian can occur.[26] The consequences for the plasma stability,[27] the ion susceptibility,[28,29] large-scale fluctuations,[30] the initial value problem,[31] or the ion drag force on dust particles[29,32,33] have been investigated. It is the purpose of this paper to study the effect on the ion-dust streaming instability. The analysis shows that the growth rates for the most unstable mode tend to be lower in the model with non-Maxwellian ions. However, they remain on a significant level over a much broader range of ion streaming velocities than in the Maxwellian case. The largest deviations occur for low ion-neutral collision rates and high Mach numbers. While in the Maxwellian case, the instability is well described by a fluid model[19,21] for a wide range of streaming velocities, kinetic effects play a more important role if the ions are non-Maxwellian and driven by an external field.

The ion susceptibilities used for the calculation of the dispersion relation are briefly reviewed in Sec. II. They are then applied to the ion-dust streaming instability in Sec. III, where the general features of the dispersion relation are investigated. The properties of the most unstable mode are examined in Sec. IV. Limitations and possible extensions of the model are discussed in Sec. V. A summary of the results is given in Sec. VI.

II. ION RESPONSE FUNCTIONS

The kinetic equation for the derivation of the ion susceptibility can be written as[27,29]

$$\frac{\partial f_\mathrm{i}}{\partial t} + \boldsymbol{v}\cdot\frac{\partial f_\mathrm{i}}{\partial \boldsymbol{r}} + \frac{q_\mathrm{i}\boldsymbol{E}}{m_\mathrm{i}}\cdot\frac{\partial f_\mathrm{i}}{\partial \boldsymbol{v}} = -\nu_\mathrm{in}[f_\mathrm{i} - n_\mathrm{i}\,\Phi_\mathrm{n}]. \tag{1}$$

Here, m_i and q_i are the ion mass and charge, $\boldsymbol{E}$ is the electric field, ν_in is the ion-neutral collision frequency, and Φ_n is the velocity distribution of the neutrals. Ion-neutral charge-exchange collisions are treated with a Bhatnagar-Gross-Krook (BGK) collision term. Small angle elastic scattering events may be ignored since they affect the ion momentum to a significantly lesser extent, see Refs. 26 and 34. Integration of f_i over the velocity yields the ion density n_i. The kinetic equation must be complemented by Poisson's equation. The reason for the different ion velocity distributions arise from the way streaming effects are introduced. This can be accomplished, e.g., through an external electric field (field driven ion flow, FD), leading to a non-Maxwellian ion distribution, or drifting neutrals (neutral driven ion flow, ND, Maxwellian distribution), see also the discussion in Ref. 33.

The first step for the calculation of the susceptibility is to determine the stationary ion distribution, $f_{\mathrm{i}0}(\boldsymbol{v}) = n_{\mathrm{i}0}\Phi_{\mathrm{i}0}(\boldsymbol{v})$. In the field driven case,[27,29] an external electric field $\boldsymbol{E}_0 = E_0\,\hat{\boldsymbol{e}}_z$ ($E_0 > 0$) is introduced that accelerates the ions in the field direction. They collide with the neutral particles, which have a Maxwellian (MW) velocity distribution

[a)]Electronic mail: kaehlert@theo-physik.uni-kiel.de

without drift, $\Phi_{\mathrm{n}}^{\mathrm{FD}}(v) = \Phi_{\mathrm{MW}}^{\perp}(v_\perp)\Phi_{\mathrm{MW}}^{z}(v_z)$. The neutral gas temperatures T_{n} in the direction parallel and perpendicular to the electric field are identical. The stationary distribution of the ions follows from Eq. (1) as $\Phi_{\mathrm{i0}}^{\mathrm{FD}}(\boldsymbol{v}) = \Phi_{\mathrm{MW}}^{\perp}(v_\perp)\Phi_{\mathrm{i0}}^{z,\mathrm{FD}}(v_z)$, where the distribution along the electric field can be written as a superposition of shifted Maxwellians[27] with an exponential weight factor

$$\Phi_{\mathrm{i0}}^{z,\mathrm{FD}}(v_z) = \int_0^\infty \exp(-x)\,\Phi_{\mathrm{MW}}^{z}(v_z - x\,v_{\mathrm{d}})\,dx. \tag{2}$$

The (mean) drift velocity is determined by the electric field and the ion-neutral collision rate as $v_{\mathrm{d}} = q_{\mathrm{i}}E_0/(m_{\mathrm{i}}\nu_{\mathrm{in}})$.

In many calculations, for the ion-dust streaming instability or the screened potential around a dust grain, the unperturbed ion distribution function is taken as a shifted Maxwellian.[19,21,35] However, in order for this to be a valid stationary solution of Eq. (1) (in the absence of external fields), the neutral gas particles should have the same distribution. In this sense, the ion drift can be seen as a consequence of neutral gas flow, $\Phi_{\mathrm{n}}^{\mathrm{ND}}(\boldsymbol{v}) = \Phi_{\mathrm{MW}}^{\perp}(v_\perp)\Phi_{\mathrm{MW}}^{z}(v_z - v_{\mathrm{d}}) = \Phi_{\mathrm{i0}}^{\mathrm{ND}}(\boldsymbol{v})$.

While the distribution functions perpendicular to the streaming direction are equivalent, the differences in the parallel direction can be quite substantial,[27,29] even for moderate (thermal) Mach numbers, $M_{\mathrm{th}} = v_{\mathrm{d}}/v_{\mathrm{th,n}}$, where $v_{\mathrm{th,n}} = (k_{\mathrm{B}}T_{\mathrm{n}}/m_{\mathrm{i}})^{1/2}$ is the thermal velocity of the neutrals. Figure 1 shows $\Phi_{\mathrm{i0}}^{z,\mathrm{FD}}(v_z)$ for various Mach numbers. It is evident that for $M_{\mathrm{th}} \gtrsim 1$, strong deviations from a shifted Maxwellian distribution occur. The distribution shows a slower exponential decay in the streaming direction and becomes much broader. Specifically, the width ("temperature") of the non-Maxwellian distribution increases with the Mach number $\propto \sqrt{1 + M_{\mathrm{th}}^2}$,[32] while the shifted Maxwellian has a constant width. A direct comparison is shown for $M_{\mathrm{th}} = 9$.

In the second step, the susceptibility must be derived from the solution of the linearized kinetic equation. In case of the shifted Maxwellian (neutral driven flow), the result can be written as[19,21,36]

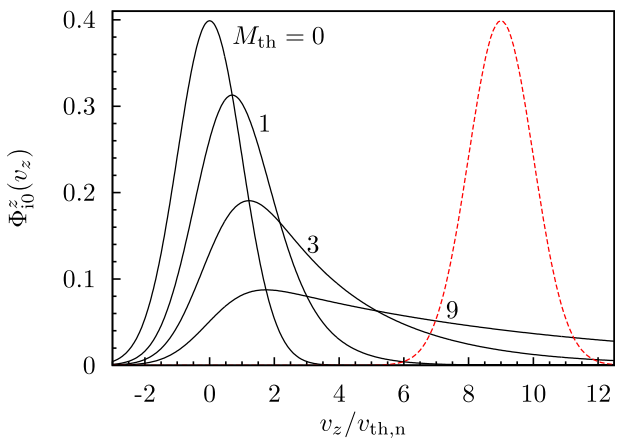

FIG. 1. Ion velocity distribution function parallel to the external electric field for different thermal Mach numbers as indicated in the figure. The full lines depict the solution of Eq. (2), while the dashed line (red) shows a shifted Maxwellian distribution.

$$\chi_{\mathrm{i}}^{\mathrm{ND}}(\boldsymbol{k},\omega) = \frac{1}{k^2\lambda_{\mathrm{Di}}^2}\frac{1 + \zeta Z(\zeta)}{1 + \dfrac{i\nu_{\mathrm{in}}}{\sqrt{2}\,k\,v_{\mathrm{th,n}}}Z(\zeta)}, \tag{3}$$

where $\lambda_{\mathrm{Di}} = v_{\mathrm{th,i}}/\omega_{\mathrm{pi}}$ is the ion Debye length, $v_{\mathrm{th,i}} = v_{\mathrm{th,n}}$ is the ion thermal speed, and the plasma dispersion function, $Z(\zeta) = i\sqrt{\pi}\exp(-\xi^2)\,\mathrm{erfc}(-i\xi)$, is evaluated at a Doppler-shifted frequency, $\zeta = (\omega + i\nu_{\mathrm{in}} - k_z v_{\mathrm{d}})/(\sqrt{2}\,v_{\mathrm{th,i}}\,k)$.

The result in the field-driven case can be expressed in a similar form[29]

$$\chi_{\mathrm{i}}^{\mathrm{FD}}(\boldsymbol{k},\omega) = \frac{(k\lambda_{\mathrm{in}})^{-2}}{1 + \dfrac{i\,k_z}{k^2 l_E}}\frac{1 + \langle\alpha(x)Z[\alpha(x)]\rangle}{1 + \dfrac{i\nu_{\mathrm{in}}}{\omega + i\nu_{\mathrm{in}}}\alpha(0)Z[\alpha(0)]}, \tag{4}$$

where the parameter $\alpha(x)$ reads

$$\alpha(x) = \frac{\omega + i\nu_{\mathrm{in}} - k_z v_{\mathrm{d}} x}{\sqrt{2}\,v_{\mathrm{th,n}}k\sqrt{1 + \dfrac{i\,k_z}{k^2 l_E}}}, \tag{5}$$

and $\lambda_{\mathrm{in}} = v_{\mathrm{th,n}}/\omega_{\mathrm{pi}}$, $l_E = m v_{\mathrm{th,n}}^2/(q_{\mathrm{i}}E_0)$. In the numerator of Eq. (4), the brackets denote an average according to $\langle f(x)\rangle = \int_0^\infty \exp(-x)f(x)dx$, which is a result of the ion velocity distribution, see Eq. (2). Additional terms compared to Eq. (3) are due to a term involving the external electric field in the linearized kinetic equation that accounts for the constant acceleration an ion experiences in the field direction. There exists an equivalent integral representation of the susceptibility,[27,29] which may also be used for a numerical implementation.

III. DISPERSION OF DUST DENSITY WAVES

In this section, the ion susceptibility will be used to study the dispersion relation of dust density waves. The general form of the dispersion relation for longitudinal plasma waves is given by the following equation:

$$\epsilon(\boldsymbol{k},\omega) = 1 + \sum_{\alpha=\mathrm{e,i,d}}\chi_\alpha(\boldsymbol{k},\omega) = 0, \tag{6}$$

where $\chi_\alpha(\boldsymbol{k},\omega)$ denotes the susceptibilities of electrons, ions, and the dust particles.

Equation (6) contains a large number of different waves such as electron plasma oscillations or ion-acoustic modes. Here, the focus will be on oscillations of the dust component. Since the frequency of dust density waves is very low compared with typical electron and ion time scales, in particular, $\omega \ll \nu_{\mathrm{in}}$, the electron and ion susceptibilities will be approximated by their static limits, $\omega = 0$. The electrons are usually much hotter than the ions and the neutral gas, $T_{\mathrm{e}} \approx$ a few eV, and electron flows are often negligible. Their susceptibility can then be approximated by $\chi_{\mathrm{e}}(\boldsymbol{k},0) \approx (k\lambda_{\mathrm{De}})^{-2}$, where λ_{De} is the electron Debye length. For the ions, the susceptibilities given in Section II are used, Eqs. (3) and (4). In the case of the dust particles, the cold-fluid approximation is employed, $\chi_{\mathrm{d}} \approx -\omega_{\mathrm{pd}}^2/\omega^2$ (dust plasma frequency ω_{pd}). This approximation is valid for $\omega/k \gg v_{\mathrm{th,d}}$, where $v_{\mathrm{th,d}}$ is the dust thermal speed, which is neglected here

to focus on the influence of the ion susceptibility on the dispersion. The same applies to dust-neutral damping. Both effects could be restored for direct comparisons with experiments at a later stage.

Based on the above approximations, the dispersion relation can now be directly solved for $\omega(\boldsymbol{k})$ with the result (see, e.g., Refs. 9 and 21)

$$\omega(\boldsymbol{k}) = \sqrt{\frac{\omega_{\mathrm{pd}}^2}{1 + (k\lambda_{\mathrm{De}})^{-2} + \chi_{\mathrm{i}}(\boldsymbol{k}, 0)}} = \omega_r + i\,\omega_i, \qquad (7)$$

where ω_r and ω_i denote the real and imaginary parts of the complex frequency, respectively. This will be the basis for the following calculations.

For a given wavenumber $k\lambda_{\mathrm{De}}$, the frequency $\omega/\omega_{\mathrm{pd}}$ depends on the ion-neutral collision rate, $\nu_{\mathrm{in}}/\omega_{\mathrm{pi}}$, the projection of the flow velocity on the wavevector normalized by the thermal speed of the neutrals, $M_{\mathrm{th}}\cos\theta$ [$\theta = \angle(\boldsymbol{k}, \boldsymbol{v}_{\mathrm{d}})$], and the parameter $\sigma = n_{\mathrm{i}0}T_{\mathrm{e}}/(n_{\mathrm{e}0}T_{\mathrm{n}})$. Note that, in general, $n_{\mathrm{i}0} \neq n_{\mathrm{e}0}$ because the dust modifies the quasi-neutrality condition due to electron collection. For low dust concentration, σ reduces to the electron-neutral temperature ratio.

A. Dispersion relation for non-Maxwellian ions

The general form of the dispersion relation for field driven ions will be investigated first. Figures 2(a) and 2(b) depict the effect of the Mach number and the angle θ. The real part of the frequency increases with the wavenumber and approaches the dust plasma frequency at short wavelengths. The initial growth becomes steeper as $M_{\mathrm{th}}\cos\theta$ is increased. The imaginary part (growth rate) [Fig. 2(b)], on the other hand, has a maximum at a finite wavenumber and goes to zero for $k \to \infty$. The maximum growth rate initially increases with $M_{\mathrm{th}}\cos\theta$, reaches a peak around $M_{\mathrm{th}}\cos\theta \approx 8$, and then drops again. At the same time, its position is shifted to longer wavelengths. Wave propagation perpendicular to the field, i.e., $M_{\mathrm{th}}\cos\theta = 0$, is a special case because the ion susceptibility is simply given by $\chi_{\mathrm{i}}^{\mathrm{FD}}(\omega = 0, k_z = 0) = (k_\perp\lambda_{\mathrm{in}})^{-2}$. Here, the wave exhibits no instability and the dispersion relation agrees with the usual dust-acoustic wave for cold dust, see Eq. (7).

The effect of the electron-neutral temperature ratio is investigated in panels (c) and (d) of Fig. 2. Increasing σ leads to a slower increase of the real part and also shifts the maximum of the growth rate, which goes along with a higher growth rate. Note that the real part can slightly exceed the dust plasma frequency.

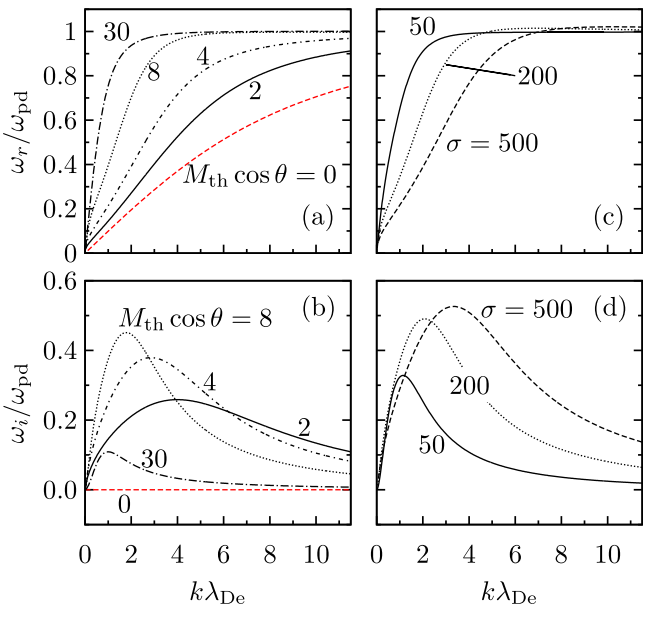

FIG. 2. Real (top) and imaginary parts (bottom) of the wave frequency for field-driven ions (non-Maxwellian) with $\nu_{\mathrm{in}}/\omega_{\mathrm{pi}} = 0.1$ and (a) and (b) $\sigma = 100$ and $M_{\mathrm{th}}\cos\theta$ as indicated in the figure. In (c) and (d), $M_{\mathrm{th}}\cos\theta = 10$.

B. Comparison with shifted Maxwellian distribution

A comparison between Maxwellian ions in the neutral driven model and the field-driven case is shown in Fig. 3. Note that in the Maxwellian model $T_{\mathrm{n}} = T_{\mathrm{i}}$. At intermediate collisionality, $\nu_{\mathrm{in}}/\omega_{\mathrm{pi}} = 0.2$ [panels (a) and (b)], the dispersion relations deviate substantially. In particular, for $M_{\mathrm{th}}\cos\theta = 4$, the Maxwellian model predicts a significantly higher growth rate and an oscillation frequency that by far exceeds the dust plasma frequency, whereas this effect is almost absent in the non-Maxwellian case (see also Fig. 2). In contrast, for $M_{\mathrm{th}}\cos\theta = 1$, the oscillation frequencies are in good agreement, while the deviations for the growth rate persist. In the high damping regime, the agreement is much better and both models yield similar results for the dispersion, see Figs. 3(c) and 3(d).

In summary, field-driven (non-Maxwellian) ions lead to features in the dispersion similar to those observed in the Maxwellian model,[6,19,21] which are, however, significantly less pronounced. This concerns, i.e., the real part of the

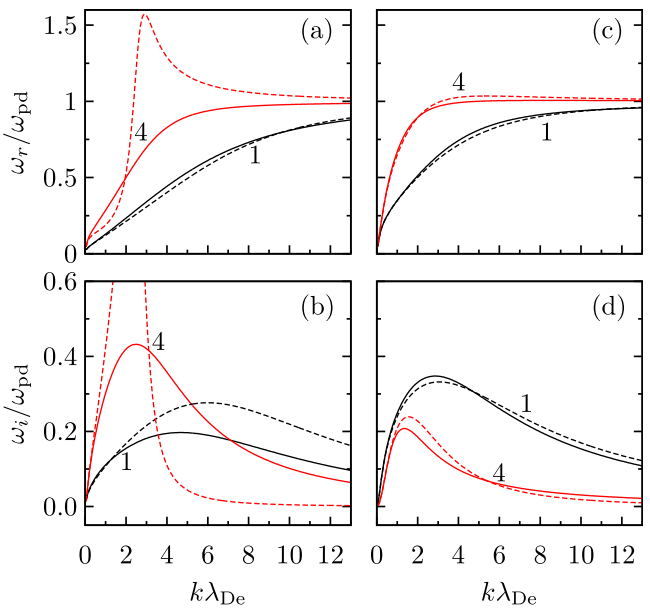

FIG. 3. Comparison of the real (top) and imaginary parts (bottom) of the dispersion relation for (a) and (b) $\nu_{\mathrm{in}}/\omega_{\mathrm{pi}} = 0.2$ and (c) and (d) $\nu_{\mathrm{in}}/\omega_{\mathrm{pi}} = 1.9$ as obtained from a shifted Maxwellian distribution (dashed line) and non-Maxwellian ions (solid line) for $\sigma = 100$. Numbers in the figure denote the values of $M_{\mathrm{th}}\cos\theta$.

frequency, which barely exceeds the dust plasma frequency, or the growth rates, which are significantly lower than in the Maxwellian model for the Mach numbers considered here (low ion-neutral damping). A more detailed investigation is presented in Section IV.

IV. PROPERTIES OF THE MOST UNSTABLE MODE

While there exist various unstable modes with different k (some modes will be stable if dust-neutral damping is included), the instability is expected to occur predominantly at the wavenumber k^* with the highest growth rate,[9,21] which thus deserves a closer inspection. The properties of this particular mode will be investigated, in detail, in the following, see also the related investigation in Ref. 21 for Maxwellian ions.

A. Wavenumber

The wavenumber k^* at which the most unstable mode occurs is shown in Fig. 4. For small ion-neutral collision rates, it is a decreasing function of $M_{\mathrm{th}}\cos\theta$, whereas for high collisionality a maximum at very small Mach numbers is observed, see the case $\nu_{\mathrm{in}}/\omega_{\mathrm{pi}} = 1.9$. While the models give similar results for high collisionality, significant deviations are found for $\nu_{\mathrm{in}}/\omega_{\mathrm{pi}} < 1$. For low Mach numbers, field driven ions typically yield smaller values for k^* than neutral driven ions. The opposite is observed for $M_{\mathrm{th}}\cos\theta \gtrsim 3-5$, depending on the ion-neutral collision frequency. More insight into the weak damping limit can be obtained by a closer inspection of the ion susceptibilities.

In the small Mach number, $M_{\mathrm{th}}\cos\theta \ll 1$, and negligible damping regime, $\nu/(k\,v_{\mathrm{th,n}}) \to 0$,[37] the ion susceptibilities can be approximated by

$$\chi_{\mathrm{i}}(\boldsymbol{k},0) \approx \frac{1}{k^2\lambda_{\mathrm{in}}^2}\left[1 - i\sqrt{\frac{\pi}{2}}M_{\mathrm{th}}\cos\theta\right], \tag{8}$$

see Refs. 4 and 36 for the Maxwellian distribution. In the non-Maxwellian case, this can be inferred, e.g., from

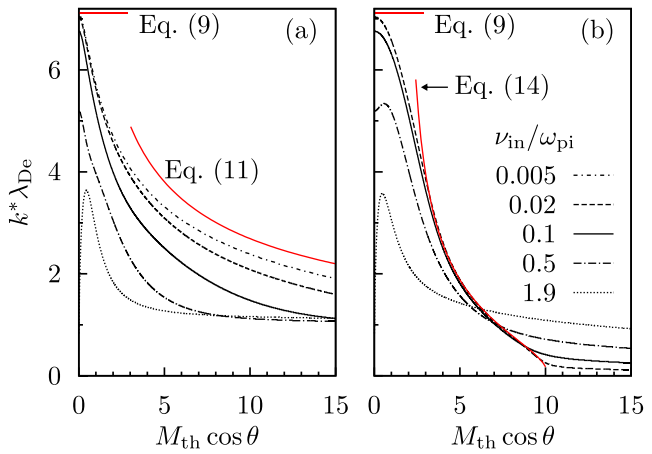

FIG. 4. Wavenumber of the mode with the highest growth rate as a function of the Mach number and the propagation angle for various damping rates $\nu_{\mathrm{in}}/\omega_{\mathrm{pi}}$ (indicated in the figure) for (a) non-Maxwellian and (b) Maxwellian ions with $\sigma = 100$. Note that the case $\nu_{\mathrm{in}}/\omega_{\mathrm{pi}} = 0.005$ is only shown in the left panel.

Eq. (15) in Ref. 27 for $M_{\mathrm{th}}\cos\theta \ll 1$. Solving Eq. (6) under the assumption $\omega_i \ll \omega_r$, and maximizing ω_i with respect to k yields the most unstable wavenumber as[3,4]

$$k^*\lambda_{\mathrm{in}} = \sqrt{\frac{1+1/\sigma}{2}}. \tag{9}$$

Equation (9) is an upper limit on the wavenumber at low Mach numbers and finite damping as can be seen in Fig. 4. The imaginary term in Eq. (8) is a small correction that drives a dust-acoustic wave unstable. For finite $M_{\mathrm{th}}\cos\theta$ and at low damping, the initial decrease of k^* is faster in the FD case.

Again neglecting all ion-neutral damping terms but retaining a finite flow velocity, the susceptibility in the FD case for $M_{\mathrm{th}}\cos\theta \gg 1$ can be roughly approximated by (see Refs. 27 and 29)

$$\chi_{\mathrm{i}}^{\mathrm{FD}}(\boldsymbol{k},0) \approx -i\sqrt{\frac{\pi}{2}}\frac{(k\lambda_{\mathrm{in}})^{-2}}{M_{\mathrm{th}}\cos\theta}. \tag{10}$$

Further neglecting the electron screening term in Eq. (7) for $\sigma \gg M_{\mathrm{th}}\cos\theta$, the location of the most unstable mode can be estimated as

$$k^*\lambda_{\mathrm{in}} \approx \left(\frac{\pi}{6}\right)^{1/4}\frac{1}{(M_{\mathrm{th}}\cos\theta)^{1/2}}. \tag{11}$$

Due to the approximations involved, the quantitative agreement of Eq. (11) with the numerical solution is not particularly good, partly because the dependence on the ion-neutral damping rate is quite strong, see Fig. 4(a). Nevertheless, Eq. (11) describes the general dependence of k^* on the Mach number for finite collisionality (up to a shift) correctly.

In the Maxwellian model, one can approximate k^* for a wide range of parameters from the relation (see Ref. 19)

$$\omega_{\mathrm{iaw}}(k^*) \approx k^*\cos\theta\, v_{\mathrm{d}}, \tag{12}$$

$$\omega_{\mathrm{iaw}}^2(k) \approx \frac{c_{\mathrm{s}}^2 k^2}{1+(k\lambda_{\mathrm{De}})^2} + 3\,k^2 v_{\mathrm{th,i}}^2, \tag{13}$$

which is similar to the resonance condition $\omega_{\mathrm{pe}} = k^*\cos\theta\, v_{\mathrm{d}}$ for the Buneman instability in an electron-ion plasma.[21,36] The electron plasma frequency ω_{pe} has been replaced by the frequency of an ion-acoustic wave, $\omega_{\mathrm{iaw}}(k)$, where $c_{\mathrm{s}} = \omega_{\mathrm{pi}}\lambda_{\mathrm{De}} = \sqrt{\sigma}\,v_{\mathrm{th,i}}$ denotes the Bohm or ion-acoustic velocity.[38] Neglecting Landau and collisional damping, Eqs. (12) and (13) correspond to the roots of the denominator in Eq. (7).

Solving Eqs. (12) and (13) for k^* leads to

$$k^*\lambda_{\mathrm{De}} \approx \sqrt{\frac{\sigma+3-(M_{\mathrm{th}}\cos\theta)^2}{(M_{\mathrm{th}}\cos\theta)^2-3}}, \tag{14}$$

which describes the behavior over a wide range of streaming velocities, $3 \lesssim M_{\mathrm{th}}\cos\theta \lesssim 10$, provided $\nu_{\mathrm{in}}/\omega_{\mathrm{pi}} \lesssim 0.1$, see Fig. 4(b). Adding the ion thermal term $\sim 3\,k^2 v_{\mathrm{th,i}}^2$ in Eq. (13) compared with Ref. 19 somewhat improves the agreement for larger wavenumbers, i.e., smaller $M_{\mathrm{th}}\cos\theta$. For lower values of $M_{\mathrm{th}}\cos\theta$, this approximation breaks down, and other

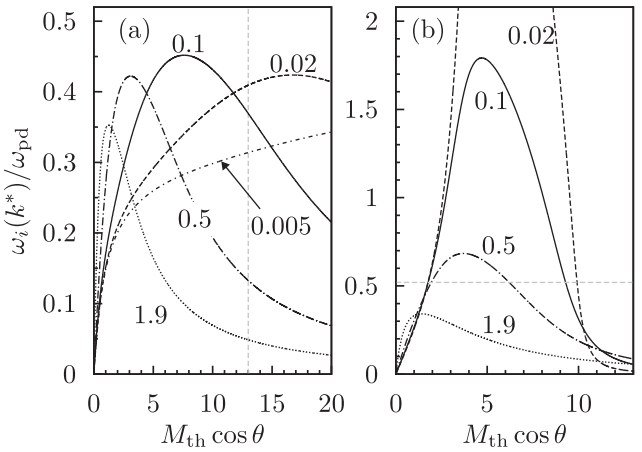

FIG. 5. Maximum growth rate as a function of the Mach number and the propagation angle for various damping rates ν_{in}/ω_{pi} (indicated in the figure) for (a) non-Maxwellian and (b) Maxwellian ions with $\sigma = 100$. Note the different scaling of the axes. The dashed lines are included as a guide for the eye and indicate the parameter ranges shown in the other panel.

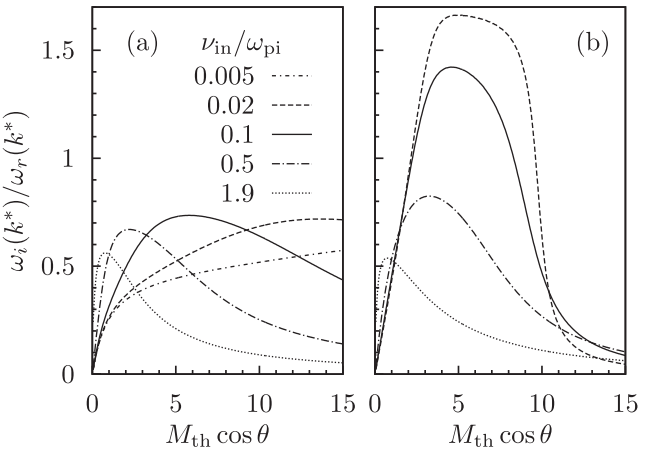

FIG. 6. Ratio of the real and imaginary parts of the most unstable mode as a function of the Mach number and the propagation angle for various damping rates ν_{in}/ω_{pi} (indicated in the figure) for (a) non-Maxwellian and (b) Maxwellian ions with $\sigma = 100$.

effects must be taken into account.[19,21] The dependence on the ion-neutral collision frequency is quite weak for the Maxwellian distribution, whereas in the non-Maxwellian case significant deviations occur between $\nu_{in}/\omega_{pi} = 0.1$ and $\nu_{in}/\omega_{pi} = 0.005$.

In summary, the largest deviations between the two models occur for weak collisionality and high Mach numbers. For typical parameters ($M_{th}\cos\theta = 8$, $\nu_{in}/\omega_{pi} = 0.1$, $\sigma = 100$), one finds $k^*_{FD}/k^*_{ND} \approx 2.4$. The wavenumber at which the most unstable mode is found roughly decreases $\sim M_{th}^{-1/2}$ for the non-Maxwellian distribution [Eq. (11)], while in the Maxwellian case Eq. (14) applies, see also Refs. 19 and 21.

B. Frequency

Figure 5 shows the maximum growth rate as a function of $M_{th}\cos\theta$ for various ion-neutral damping rates. Note the different scaling of the axes for field-driven [Fig. 5(a)] and neutral-driven ions [Fig. 5(b)]. In both models, there exists a maximum (see also Ref. 21 for Maxwellian ions), which is shifted to lower values of $M_{th}\cos\theta$ as the ion-neutral collision frequency becomes larger, see also Fig. 2(b). The agreement between the models is good in the high damping limit, $\nu_{in}/\omega_{pi} = 1.9$ (see also Fig. 3), whereas rather large deviations are observed at lower damping. Consider, in particular, the transition $\nu_{in}/\omega_{pi} = 0.1 \to 0.02$. While the growth rates in the Maxwellian model increase further [roughly $\sim(\omega_{pi}/\nu_{in})^{1/2}$ for the Buneman-type instability[19]] and show a very strong dependence on the Mach number with a steep drop around $M_{th}\cos\theta \approx 10$ (related to the Bohm speed, see Fig. 4), the model with field-driven ions predicts that even for larger values of $M_{th}\cos\theta$ significant growth rates can occur. This is especially apparent for $\nu_{in}/\omega_{pi} = 0.005$. Figure 5 can further be used to determine if the highest growth rate is found in the flow direction or under an oblique angle[6,21] for a fixed Mach number M_{th}. Since $M_{th}\cos\theta$ can assume all values up to M_{th}, the former occurs if M_{th} found to the left of the maximum, while the latter occurs in the opposite case.

The ratio between the imaginary and real parts of the wave frequency at the wavenumber with the highest growth rate is shown in Fig. 6. While in the Maxwellian case, the imaginary part exceeds the real part for low to intermediate ion-neutral damping and Mach numbers in the range $3 \lesssim M_{th}\cos\theta \lesssim 10$, largely different behavior is observed for non-Maxwellian ions. Here, the oscillation frequency (real part) exceeds the growth rate, regardless of the Mach number and the collisionality, i.e., the instability grows relatively slowly. The model with Maxwellian ions shows this behavior only at high ion-neutral damping.

C. Discussion

The velocity distribution plays a major role in determining the properties of the instability. While it becomes much broader at higher Mach numbers in the field-driven model, the width of the shifted Maxwellian for neutral-driven ions remains constant. Thus, instead of being peaked at the streaming velocity with a small thermal spread, the velocity distribution has finite values in a much broader range (see Fig. 1).

One can see from Refs. 19 and 21 and the discussion in Sec. IV A that the wavenumber k^* for neutral driven ions can be well described by a hydrodynamic model for not too small $M_{th}\cos\theta$. On the other hand, the origin of Eq. (10), which roughly describes the wavenumber of the instability in the FD model for $M_{th}\cos\theta \gg 1$, is kinetic.[29] Thus, compared with the Maxwellian model, where hydrodynamic effects dominate in this regime, kinetic contributions have a higher weight in the field driven case. Note that the approximation of the ion susceptibility for $M_{th}\cos\theta \gg 1$, Eq. (10), contains the same kinetic term as in the limit $M_{th}\cos\theta \ll 1$ [Eq. (8)], the only difference being the scaling with the Mach number. However, the ion Debye screening term $\sim(k\lambda_{in})^{-2}$ is missing in Eq. (10). Ion-neutral damping has been neglected in this analysis and leads to a downshift of k^* and considerably affects the growth rates.

V. DISCUSSION OF THE MODEL

In this section, some of the drawbacks and restrictions of the theory will be discussed.

The BGK collision operator employed in the calculation of the ion response function assumes a constant ion collision frequency. It was shown[26] that this approximation yields good results for the ion distribution at small Mach numbers when compared with Monte Carlo simulations based on energy dependent cross sections. Deviations occurred for higher Mach numbers, where the simulations showed a Gaussian instead of an exponential tail. However, the constant ν_{in} approximation does capture the broadening of the distribution and its asymmetry, which is missing if a shifted Maxwellian is used. Furthermore, the kinetic equations can be solved analytically. Therefore, using the BGK collision operator is a practical method to include the dominant effects of ion-neutral collisions. An alternative solution would be the assumption of a constant mean free path,[27] which admits an analytical solution of the kinetic equation in the case of cold neutrals. The corresponding distribution function for the ions shows similar broadening as in the constant ν_{in} case, which is the main difference compared to the shifted Maxwellian. Therefore, one may expect that the instability is affected similarly.

The theory assumes that the electric field is constant, whereas in experiments the field strength may vary, especially in the sheath region. This was shown to affect, e.g., the screening of the dust potential.[39] Thus, the theory here should be applicable if the electric field varies only weakly across the extension of the dust cloud. At low collisionality and for strong variations of the electric field, infrequent collisions may further hinder (local) equilibration and cause deviations from a distribution based on the assumption $\boldsymbol{E}_0 = \mathrm{const}$.

It was shown[27] that field-driven ions can become unstable at low ion-neutral damping and high Mach numbers, which would affect their screening properties and, thus, the development of the ion-dust instability. The parameter range, where the ion instability occurs when electron screening is included, was estimated roughly as $8 \lesssim M_{\mathrm{th}} \lesssim \sqrt{T_{\mathrm{e}}/T_{\mathrm{n}}}$ and $\nu_{\mathrm{in}}/\omega_{\mathrm{pi}} \lesssim 0.3$. For the parameters studied here with $\sqrt{T_{\mathrm{e}}/T_{\mathrm{n}}} \approx 10$, it can thus be expected that if the instability occurs, then only in a small region of the parameter space. This might further be affected by the presence of (large amounts of) dust in the plasma. A detailed investigation of these questions is beyond the scope of this paper.

The dispersion relation, Eq. (7), neglects some of the effects that could be important in a realistic experimental situation,[22,25] e.g., dust-neutral damping, dust-thermal effects, charge fluctuations, or drifts of other components.[17] Strong coupling effects of the dust component[40] could also play a role. More sophisticated expressions for the dielectric function can be constructed if necessary. Moreover, dust density waves observed in experiments often have significant amplitudes (e.g., Refs. 41 and 42), i.e., they are not strictly in the linear regime. Thus, a nonlinear treatment of the wave would be preferable compared to the linear theory presented here. Nevertheless, the linear theory is a valuable tool to investigate the stability of the system and valid in the initial phase before the wave becomes nonlinear. The present calculations could partially be extended into the nonlinear regime through molecular dynamics simulations of the dust particles as was done in Refs. 24 and 43, where the ion susceptibility was used as input for the calculation of a (linearly) screened dust interaction. This would automatically include some of the effects also missing in the linear theory such as dust thermal and strong coupling effects.

VI. CONCLUSION

The comparison between the models with field-driven (non-Maxwellian) and neutral-driven (Maxwellian) ions shows that the latter lead to more pronounced features in the dispersion relation of dust density waves, such as higher growth rates or oscillation frequencies far above the dust plasma frequency, albeit in a limited range of drift speeds. At low ion-neutral damping rates, field-driven ions lead to significant growth rates even beyond the Bohm speed, whereas the growth rates quickly decrease in this regime for Maxwellian ions. In the high damping limit, both models yield similar results. Kinetic effects play an important role in the field-driven model even for high Mach numbers, while in the Maxwellian case a fluid model yields similar results.[21] Since the deviations can be quite substantial, non-Maxwellian distribution functions could be another factor to consider when the effects of different physical processes on the dispersion relation are investigated.[25]

ACKNOWLEDGMENTS

I would like to thank P. Ludwig, J.-P. Joost, and M. Bonitz for stimulating discussions. This work was supported by the DFG via SFB-TR24, Project A7.

[1]N. Rao, P. Shukla, and M. Y. Yu, Planet. Space Sci. **38**, 543 (1990).
[2]A. Barkan, R. L. Merlino, and N. D'Angelo, Phys. Plasmas **2**, 3563 (1995).
[3]V. Molotkov, A. Nefedov, V. Torchinskii, V. Fortov, and A. Khrapak, J. Exp. Theor. Phys. **89**, 477 (1999).
[4]V. E. Fortov, A. G. Khrapak, S. A. Khrapak, V. I. Molotkov, A. P. Nefedov, O. F. Petrov, and V. M. Torchinsky, Phys. Plasmas **7**, 1374 (2000).
[5]E. Thomas, Phys. Plasmas **13**, 042107 (2006).
[6]A. Piel, M. Klindworth, O. Arp, A. Melzer, and M. Wolter, Phys. Rev. Lett. **97**, 205009 (2006).
[7]M. Schwabe, M. Rubin-Zuzic, S. Zhdanov, H. M. Thomas, and G. E. Morfill, Phys. Rev. Lett. **99**, 095002 (2007).
[8]S. V. Annibaldi, A. V. Ivlev, U. Konopka, S. Ratynskaia, H. M. Thomas, G. E. Morfill, A. M. Lipaev, V. I. Molotkov, O. F. Petrov, and V. E. Fortov, New J. Phys. **9**, 327 (2007).
[9]T. M. Flanagan and J. Goree, Phys. Plasmas **17**, 123702 (2010).
[10]T. M. Flanagan and J. Goree, Phys. Plasmas **18**, 013705 (2011).
[11]J. D. Williams, Phys. Plasmas **19**, 113701 (2012).
[12]Y.-Y. Tsai and L. I, Phys. Rev. E **90**, 013106 (2014).
[13]R. L. Merlino, J. Plasma Phys. **80**, 773 (2014).
[14]N. D'Angelo and R. L. Merlino, Planet. Space Sci. **44**, 1593 (1996).
[15]A. A. Mamun and P. K. Shukla, Phys. Plasmas **7**, 4412 (2000).
[16]V. V. Yaroshenko, B. M. Annaratone, S. A. Khrapak, H. M. Thomas, G. E. Morfill, V. E. Fortov, A. M. Lipaev, V. I. Molotkov, O. F. Petrov, A. I. Ivanov, and M. V. Turin, Phys. Rev. E **69**, 066401 (2004).
[17]V. V. Yaroshenko, S. A. Khrapak, H. M. Thomas, and G. E. Morfill, Phys. Plasmas **19**, 023702 (2012).
[18]M. Rosenberg, Planet. Space Sci. **41**, 229 (1993).
[19]M. Rosenberg, J. Vac. Sci. Technol. A **14**, 631 (1996).
[20]M. Rosenberg, J. Plasma Phys. **67**, 235 (2002).

[21]A. Piel, O. Arp, M. Klindworth, and A. Melzer, Phys. Rev. E **77**, 026407 (2008).
[22]M. Rosenberg, E. Thomas, and R. L. Merlino, Phys. Plasmas **15**, 073701 (2008).
[23]D. Winske and M. Rosenberg, IEEE Trans. Plasma Sci. **26**, 92 (1998).
[24]G. Joyce, M. Lampe, and G. Ganguli, Phys. Rev. Lett. **88**, 095006 (2002).
[25]W. D. S. Ruhunusiri and J. Goree, Phys. Plasmas **21**, 053702 (2014).
[26]M. Lampe, T. B. Röcker, G. Joyce, S. K. Zhdanov, A. V. Ivlev, and G. E. Morfill, Phys. Plasmas **19**, 113703 (2012).
[27]R. Kompaneets, A. V. Ivlev, S. V. Vladimirov, and G. E. Morfill, Phys. Rev. E **85**, 026412 (2012).
[28]V. Schweigert, Plasma Phys. Rep. **27**, 997 (2001).
[29]A. V. Ivlev, S. K. Zhdanov, S. A. Khrapak, and G. E. Morfill, Phys. Rev. E **71**, 016405 (2005).
[30]A. I. Momot and A. G. Zagorodny, Phys. Plasmas **18**, 102110 (2011).
[31]R. Kompaneets, Y. O. Tyshetskiy, and S. V. Vladimirov, Phys. Plasmas **20**, 042108 (2013).
[32]L. Patacchini and I. H. Hutchinson, Phys. Rev. Lett. **101**, 025001 (2008).
[33]I. H. Hutchinson and C. B. Haakonsen, Phys. Plasmas **20**, 083701 (2013).
[34]A. V. Phelps, J. Appl. Phys. **76**, 747 (1994).
[35]P. Ludwig, W. J. Miloch, H. Kählert, and M. Bonitz, New J. Phys. **14**, 053016 (2012).
[36]A. A. Rukhadze, A. F. Alexandrov, and L. S. Bogdankevich, *Principles of Plasma Electrodynamics* (URSS, Moscow, 2013).
[37]It is still assumed that the ions adjust instantaneously to the dust motion, even though ion-neutral damping is neglected.
[38]P. M. Bellan, *Fundamentals of Plasma Physics* (Cambridge University Press, 2006).
[39]R. Kompaneets, A. V. Ivlev, V. Nosenko, and G. E. Morfill, Phys. Rev. E **89**, 043108 (2014).
[40]M. Rosenberg, G. J. Kalman, P. Hartmann, and J. Goree, Phys. Rev. E **89**, 013103 (2014).
[41]L.-W. Teng, M.-C. Chang, Y.-P. Tseng, and L. I, Phys. Rev. Lett. **103**, 245005 (2009).
[42]R. L. Merlino, J. R. Heinrich, S.-H. Hyun, and J. K. Meyer, Phys. Plasmas **19**, 057301 (2012).
[43]M. Lampe, G. Joyce, and G. Ganguli, IEEE Trans. Plasma Sci. **33**, 57 (2005).